

Aerosol Science and Technology 30:40-61 (1999)  
©1999 American Association for Aerosol Research  
Published by Taylor and Francis  
0278-6826/99 \$12.00 + .00



## The DMA Transfer Function with Brownian Motion a Trajectory/Monte-Carlo Approach

*Charles Hagwood, Yudaya Sivathanu\*, and George Mulholland*

STATISTICAL ENGINEERING DIVISION, NATIONAL INSTITUTE OF STANDARDS  
AND TECHNOLOGY, GAITHERSBURG, MD (C. H.), DEPARTMENT OF MECHANICAL  
ENGINEERING, PURDUE UNIVERSITY, WEST LAFAYETTE, IN (Y. S.), FIRE  
MEASUREMENT AND RESEARCH DIVISION, NATIONAL INSTITUTE OF STANDARDS  
AND TECHNOLOGY, GAITHERSBURG, MD (G. M.)

# The DMA Transfer Function with Brownian Motion a Trajectory/Monte-Carlo Approach

*Charles Hagwood, Yudaya Sivathanu\*, and George Mulholland*

STATISTICAL ENGINEERING DIVISION, NATIONAL INSTITUTE OF STANDARDS  
AND TECHNOLOGY, GAITHERSBURG, MD (C. H.), DEPARTMENT OF MECHANICAL  
ENGINEERING, PURDUE UNIVERSITY, WEST LAFAYETTE, IN (Y. S.), FIRE  
MEASUREMENT AND RESEARCH DIVISION, NATIONAL INSTITUTE OF STANDARDS  
AND TECHNOLOGY, GAITHERSBURG, MD (G. M.)

---

**ABSTRACT.** The transfer function for the Differential Mobility Analyzer (DMA) is derived based on particle trajectories for both nondiffusing particles and diffusing particles. The effect of particle diffusion is assessed by using a Monte-Carlo method for particles of sizes 1, 3, 10, 30, and 100 nm. This approach includes both the effect of wall losses and axial diffusion. The range of validity of the Stolzenburg analysis is assessed by comparing his transfer function, the peak of his transfer function, and its dimensionless width with similar calculations based on the Monte-Carlo. For particle sizes smaller than 10 nm, the Monte-Carlo method indicates large wall losses, which result in a reduction in the peak of the transfer function by as much as a factor of 10 to 30, sensitivity to the flow-field, and skewness of the transfer function. It is shown that Stolzenburg's approximate formula for the standard deviation of the width of the transfer function agrees with Monte-Carlo simulations for particle sizes of 3 nm and larger.

---

## INTRODUCTION

The Differential Mobility Analyzer (DMA) is widely used for sizing and classifying submicrometer aerosols. The most widely used DMA is based on the design developed by Liu and Pui (1974). Recent modifications of the classifier include a rapid scanning capability, where a complete spectrum can be obtained in as fast as 30 s Wang and Flagan 1990; Endo et al. (1997),

and a radial DMA by Zhang et al. (1995) for the characterization of ultra-fine aerosols.

A clear and elegant exposition of the workings of the DMA was presented by Knutson and Whitby (1975). They model the DMA in terms of integrated functions, the stream function, and an electrical flux, rather than using the particle trajectories. Their main result is the derivation of the transfer function, defined as the probability that an aerosol particle that enters at the inlet slit will exit via the sampling slit. The beauty of their method is that the transfer function is expressed in terms of measurable quantities,

---

\* This work was partially done while Yudaya Sivathanu was visiting the Statistical Engineering Division of the National Institute of Standards and Technology as a visiting scholar with additional support from an NIST grant.

including flow rates and the electrode voltage. The transfer function is needed for inferring the size distribution of polydisperse aerosols from measurements of particle concentration versus voltage for particles exiting the classifier.

Stolzenburg (1988) extended the Knutson-Whitby analysis to the case of diffusing particles making use of an expansion about a "particle" stream function with no diffusion. Unfortunately his excellent study has not been published in a refereed journal. Independently, Tammet (1970) analytically calculated the effect of particle diffusion on the DMA transfer function. The analysis of diffusional effects in a shortened DMA by Roswell-Llompert et al. (1996) provides an overview of these two studies. The study by Zhang et al. (1996) contains explicit expressions of the transfer equation in terms of four dimensionless quantities, though one must refer to Stolzenburg's thesis to obtain an explicit expression for the diffusional spreading for the cases of plug flow and fully developed viscous flow.

The great advantage of the analysis by Stolzenburg is its generality. One can assess the effect of diffusion on the transfer function as a function of the particle size, the flow ratio through the classifier, and the length of the classifier. However, there are several issues not resolved by this analysis. One issue is a realistic description of the flow through the classifier, especially the inlet and outlet region. Chen and Pui (1997) have obtained results on the flow within the classifier for nanometer aerosol particles. Using a three-dimensional (3-D) flow code, they find for the standard DMA design that a flow recirculation develops in the DMA inlet for a 20:1 flow ratio of sheath air flow to aerosol flow. The recirculation is not present for a 10:1 ratio of flows, which is the most widely used condition. A second effect is the effect of fringing of the electrical field, again near the inlet and outlet. There is also modeling evidence of penetration of the electrical field into the aerosol inlet (Chen and Pui 1997); a detailed model of the field in the vicinity of the out-

let with multiple holes has not been developed. The third effect concerns the modeling of the diffusion with wall losses and streamwise diffusion included. Rosell-Llompert et al. (1996) include streamwise diffusion in their analysis of the optimal length of a DMA based on a delta function initial position of the aerosol. The approach of Chen and Pui (1997) is the only model that includes wall losses. A major focus of our study is the use of the Monte-Carlo method for assessing the influence of streamwise diffusion and wall losses on the transfer function. Our Monte-Carlo approach is compared to the analysis of Stolzenburg. We include the resulting equations from Stolzenburg's thesis for making the comparison.

There are two reasons for needing an improved understanding of the effect of diffusion on the transfer function: to quantify the resolution of the particle size distribution and to quantify the accuracy of the electrical mobility measurements. The driving force in the first case is the need for accurate measurements of the widths of narrow size distributions. Such measurements are important in the development of monodisperse spheres synthesized by emulsion polymerization. The specific issue addressed is the effect of particle diffusion on size resolution as a function of the ratio of the aerosol flow to the sheath flow. In the second case, the concern is the accuracy of the DMA measurement for the mean particle size. This is important for the application of the DMA for sizing measurements of particle size calibration standards such as the 100 nm particle standard issued by NIST (NIST Standard Reference Material 1963). The specific issue is the effect of particle diffusion on sizing accuracy as a function of flow ratio. Because we are using the Monte-Carlo method to investigate diffusional effects on the transfer function, our approach is trajectory based. We set up a model flow condition of plug and parabolic and explicitly define the inlet and outlet condition. These conditions are implicit in the work of Stolzenburg. First, it is shown that when the diffusion coefficient

equals zero, both the trajectory approach and the Knutson-Whitby approach give the same transfer function.

### THE DMA

Figure 1 contains a schematic of the actual classifier as well as a simplified version of it. The classifying region is bounded by a stainless steel outer cylinder with an inner radius of length  $r_2$  and a coaxial, stainless steel center rod with a radius  $r_1$ . The center rod is maintained at a voltage of  $V_0$ , and the outer cylinder is grounded. Thus, an electric field,  $\vec{E}(r, \theta, z)$ , is established in the annular region between the two cylinders.

Clean sheath air flows through the annular region along the center rod with velocity profile  $\vec{u}(r, \theta, z)$ . A smaller, polydisperse aerosol flow enters through an axisymmetric opening along the outer cylinder. The two flows meet without mixing and then flow through the classifying region. Near the bottom of the classifying region, a slit on the center rod extracts a fraction of the air flow consisting of nearly monodisperse (single-sized) aerosol particles. The remainder of the air flow exits through the end of the annular region as excess air. The length of the classifying region,  $L$ , is defined as the axial distance from the aerosol entrance to the aerosol exit at the slit in the center rod. The instrument settings are listed in Table 1.

The flow pattern inside the actual classifier is complicated. A simplified flow pattern is illustrated in Figure 1b. One can model the flow as either plug flow or fully developed parabolic

flow. Inlet and outlet slits are depicted in the figure, but these should be viewed as virtual slits. That is, they have no effect on the flow. The inlet boundary simply represents the fact that all of the aerosol is in the outer cylindrical region. The radii  $r_a$  and  $r_b$  are chosen so that a certain fraction of the flow goes through the inlet slit and an equal fraction of the flow goes through the outlet slit. Of course, the slit widths will be different for the two types of flows. None of the possible complications, such as shear flow and vortex formation, that might occur in an actual inlet or outlet are included in this analysis. If there is no diffusion, the transfer function is the same for these two flows; in fact, it is independent of flow provided the flow is laminar. Here we compute the transfer function for these same two flows, but including the effect of particle diffusion.

Our analysis was carried out for particle diameters,  $d_p$ , of 1, 3, 10, 30, and 100 nm with corresponding diffusion coefficients,  $D$ , of  $5.37 \times 10^{-2}$  cm<sup>2</sup>/s,  $5.99 \times 10^{-3}$  cm<sup>2</sup>/s,  $5.47 \times 10^{-4}$  cm<sup>2</sup>/s,  $6.42 \times 10^{-5}$  cm<sup>2</sup>/s and  $6.80 \times 10^{-6}$  cm<sup>2</sup>/s. We have used the following expression for the Cunningham slip correction:

$$C(d_p) = 1 + K_n[1.142 + 0.558e^{-0.999/K_n}],$$

where  $K_n$  is the Knudsen number ( $K_n = 2\lambda/d_p$ ) with mean free path  $\lambda = 67.43$  nm.

### THE TRAJECTORY METHOD

Monte-Carlo simulations is the tool we use to understand the DMA transfer function of diffusing aerosol particles. The Knutson and Whitby (1975) approach that uses streamlines to model the passage of an aerosol particle through the DMA classifier does not lend itself easily to Monte-Carlo simulations. Instead, a trajectory model is needed for Monte-Carlo simulations. In this section we present a trajectory approach for analyzing the DMA classifier and show how it leads to the same exact expression for the non-diffusive transfer function as that in the streamline method.

TABLE 1. DMA settings<sup>a</sup>.

|                       |  |
|-----------------------|--|
| Inner radius          | $r_1 = 0.947$ cm   |
| Outer radius          | $r_2 = 1.958$ cm   |
| Cylinder length       | $L = 44$ cm  |
| Aerosol flow          | $Q_a = 16.67$ cm <sup>3</sup> /s<br>and $4.167$ cm <sup>3</sup> /s |
| Sheath or excess flow | $Q_c = 166.67$ cm <sup>3</sup> /s                                  |

<sup>a</sup>The geometric values given in Table 1 are slightly different from the TSI DMA values with  $r_1 = 0.937$  cm,  $r_2 = 1.958$  cm and  $L = 44.44$  cm. The value of  $L/\ln(r_2/r_1)$  is 60.57 for Table 1, compared to 60.30 for the TSI values.

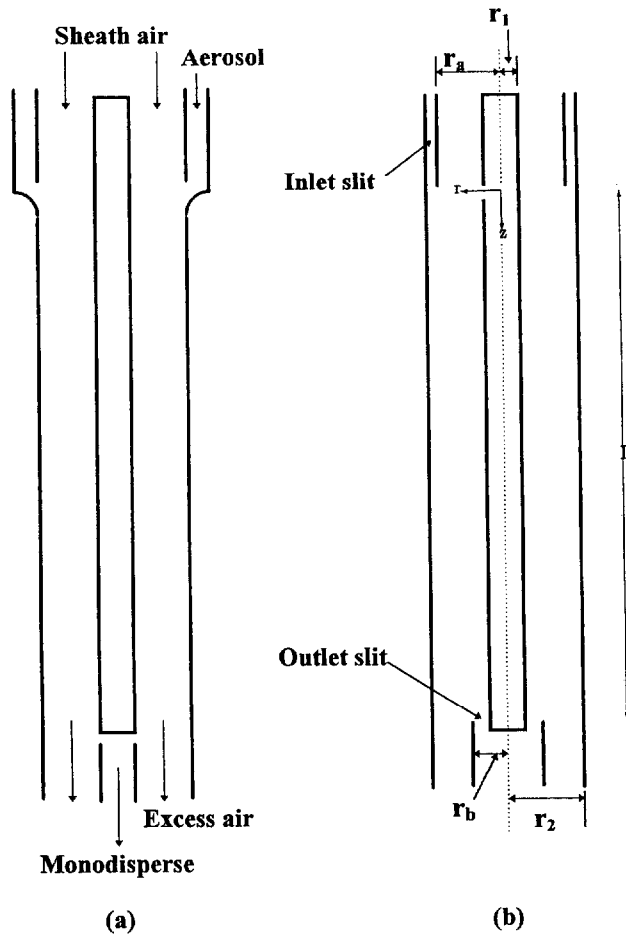


FIGURE 1. Schematic of the DMA classifier (a) and the simplified version (b) used in the calculations.

We assume that the airflow is axisymmetric, laminar, and incompressible, as done in Knutson and Whitby (1975). Let  $u_r(r, z)$  and  $u_z(r, z)$  denote the radial and axial components of the airflow velocity. Similarly, let  $E_r(r, z)$  and  $E_z(r, z)$  denote the radial and axial components of the electric field. Neglecting particle inertia and Brownian motion, the particle trajectory is described by the system of differential equations

$$\frac{dr}{dt} = u_r(r, z) + Z_p E_r(r, z), \quad (1)$$

$$\frac{dz}{dt} = u_z(r, z) + Z_p E_z(r, z), \quad (2)$$

where  $Z_p$  denotes the particle's electric mobility and is given by

$$Z_p = \frac{\epsilon C(d_p)}{3\pi\mu d_p},$$

$\epsilon$  is the charge of the electron, and  $\mu$  is the air viscosity. Particle inertia is neglected in this analysis. The validity of this approximation is evident from considering 100 nm spheres, which have a relaxation time of  $9 \times 10^{-8}$  s. The maximum aerosol velocity is of the order of 40 cm/s, which corresponds to a stopping distance of 40 nm for the 100 nm particles and even smaller stopping distances for the other sizes. Thus the particle inertia can be neglected.

Implicit in writing the equations in this form is the assumption that the flow is steady; that is, there is no time dependence in the velocity. This assumption rules out the possibility of vortex dynamics at the entrance and exit slits of the analyzer. The steady flow assumption, for this application, is equivalent to saying the flow is laminar.

The electric field for concentric cylinders (as the classifier) is given by

$$E_r(r, z) = E_r(r) = -\frac{V_0}{r \ln(r_2/r_1)},$$

$$E_z(r, z) = 0.$$

The transfer function, denoted by  $\Omega(cZ_p)$ , can now be defined as

$\Omega(cZ_p)$  = the probability that an aerosol particle which enters the DMA at the inlet will leave via the sampling slit.

$c$  is a constant depending on the electric field, specified later. Inherent in the definition is the fact that when the particle intersects the wall of the cylinder it sticks.

The probabilistic nature of the nondiffusive transfer function is a result of the random inlet distribution of particles entering the classifier. For the diffusive transfer function, diffusion is another source of randomness. Analysis based on the particle's trajectory requires that the entrance probability be a function of radial location. Particles enter the sampling region from a random radial location  $(R, 0)$ , where  $r_a \leq R \leq r_2$  and  $R$  has probability density function which depends on the velocity profile at the inlet. For example, for a uniform velocity profile this probability density function is given by  $p_{\text{plug}}(R) = 2\pi R U_0 / Q_a = 2R / (r_2^2 - r_a^2)$ ;  $U_0$  is the mean axial flow velocity and  $Q_a$  is the aerosol flow rate. For a general velocity profile,  $R$  will have probability density function given by

$$p_{\text{gen}}(R) = 2\pi R u_z(R, 0) / Q_a, \quad r_a \leq R \leq r_2. \quad (3)$$

Here we assume that  $u_z(R, 0) \geq 0$ . This distributional assumption is consistent with Knutson's and Whitby's uniform initial condition based on streamlines.

Introduce an  $r, z$ -coordinate system within the spectrometer, as shown in Fig. 1, with the positive  $z$  axis pointing in the direction of the flow, and let  $\tau$  be the solution of the equation

$$z(\tau) = L, \quad t > 0$$

given that the particle starts at  $(R, 0)$ .  $z(\tau)$  is the  $z$ -component of the aerosol particle's motion when it first reaches a position parallel to the sampling slit. The particle passes through the sampling slit at time  $\tau$  if and only if

$$r_1 < r(\tau) < r_b;$$

i.e., the radial component lies between the coordinates of the sampling slit. The transfer function is thus the probability

$$\Omega(cZ_p) = P[r_1 < r(\tau) < r_b]. \quad (4)$$

As illustrative examples, we consider the inviscid flow and the viscous flow. For inviscid (plug) flow,  $u_r(r, z) = 0$ ,  $u_z(r, z) = U_0$ ,  $E_r(r, z) = -V_0/r \ln(k)$ ,  $k = r_2/r_1$ , and  $E_z(r, z) = 0$ . Substituting into Equations (1 and 2) gives the following differential equations describing the trajectory of an aerosol particle in a plug flow:

$$\frac{dr}{dt} = -\frac{Z_p V_0}{r \ln(k)}, \quad (r(0), z(0)) = (R, 0),$$

$$\frac{dz}{dt} = U_0.$$

It is easily shown that these separable equations have solutions

$$r(t) = \sqrt{R^2 - \frac{2Z_p V_0}{\ln(k)} t}, \quad (5)$$

$$z(t) = U_0 t. \quad (6)$$

For viscous flow,  $u_r(r, z) = 0$  and the axial component of air flow satisfies

$$u_z(r) = Ar^2 + B \ln(r) + C, \quad (7)$$

$$A = \frac{1}{4\mu} \frac{dp}{dz}, \quad (8)$$

$$B = -\frac{1}{4\mu} \frac{dp}{dz} \frac{r_2^2 - r_1^2}{\ln(r_2/r_1)}, \quad (9)$$

$$C = \frac{1}{4\mu} \frac{dp}{dz} \left[ \frac{r_2^2 - r_1^2}{\ln(r_2/r_1)} \ln(r_1) - r_1^2 \right], \quad (10)$$

where  $\mu$  is the viscosity of air and  $\frac{dp}{dz}$  denotes the constant pressure gradient. Although not given here, similarly, the equation of motion of an aerosol particle in a viscous flow can be solved explicitly.

Illustrative trajectories are given in Figure 2 for plug flow with the sheath and aerosol flows of 166.7 cm<sup>3</sup>/s and 16.7 cm<sup>3</sup>/s, respectively. Figure 3 contains particle trajectories for the vis-

cus case. The zero velocity condition on the wall for the viscous flow causes the flattening of the trajectories near the inner and outer walls. The inlet and outlet widths are chosen so that there is no discontinuity in the axial velocity profiles. The inlet and outlet widths are greater for the viscous flow because of the zero velocity at walls. For plug flow all three trajectories shown in Figure 2 have the same residence times within the classifier of about 550 ms. As indicated in Figure 4, plots of time versus axial location for the viscous case, the shape of the curve and total residence time depends on the starting location and varies from about 470 ms to about 530 ms. Even though the velocity vanishes at the walls, the particles spend more time in the central region of the classifier, leading to a shorter residence time than for the plug flow.

Consider the trajectory approach for plug flow. For plug flow  $\tau = L/U_0$ , as can be seen

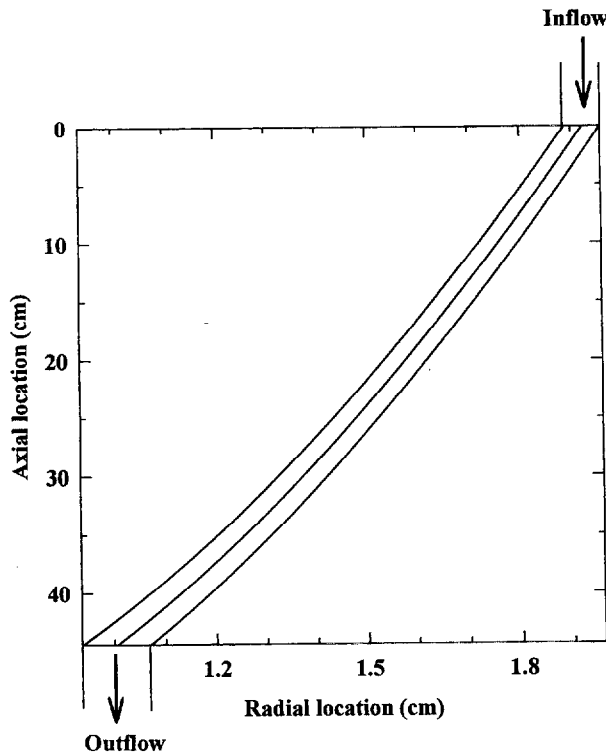


FIGURE 2. The innermost, central, and outermost particle trajectories for a DMA classifier with plug flow.

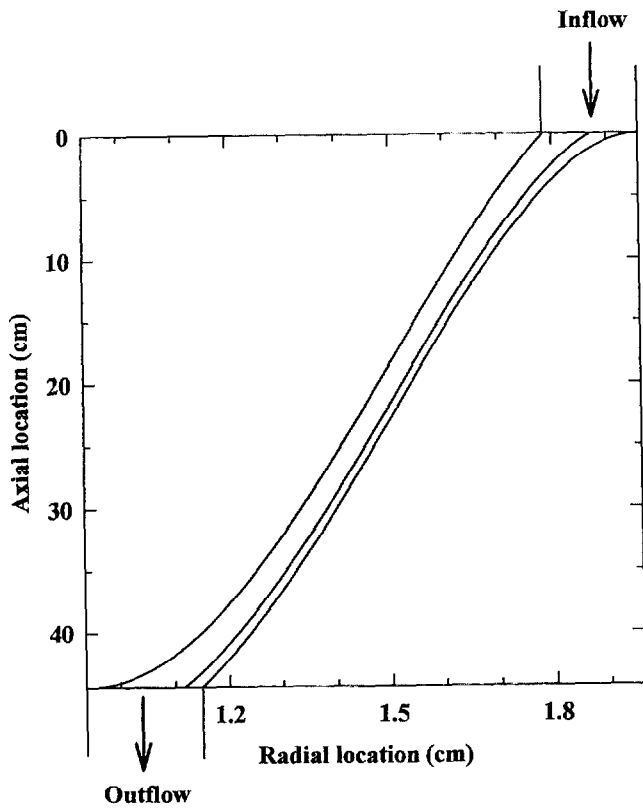


FIGURE 3. The innermost, central, and outermost particle trajectories for a DMA classifier with viscous flow.

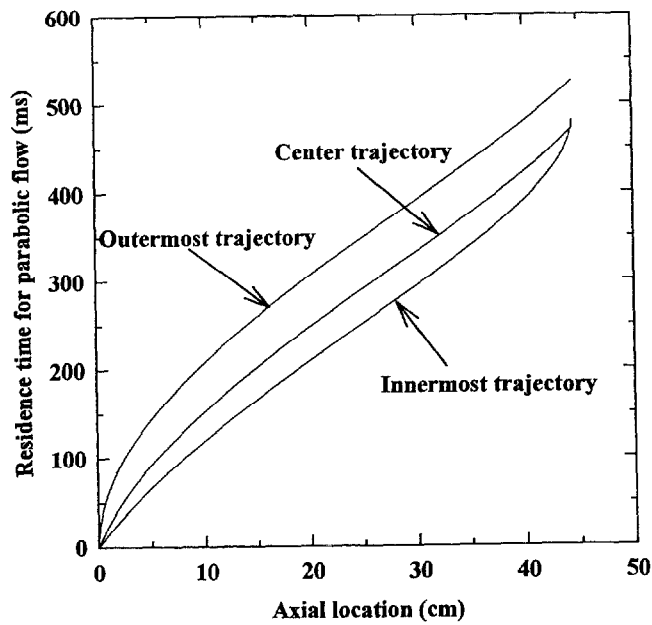


FIGURE 4. The residence times for the three trajectories for a DMA classifier with viscous flow.

from Equation (6). Starting with Equation (5), substituting this expression for  $r(\tau)$  in Equation (4), and squaring both sides of the inequality gives

$$\begin{aligned} \Omega(\Delta\Phi_0 Z_p) &= Pr[r_1 < r(L/U_0) < r_b] \\ &= Pr\left[r_1^2 + \frac{2Z_p V_0 L}{\ln(k) U_0} < R^2 < r_b^2 + \frac{2Z_p V_0 L}{\ln(k) U_0}\right], \end{aligned} \quad (11)$$

where  $\Delta\Phi_0 = -\frac{V_0}{\ln(k)}L$ ,  $k = r_2/r_1$ . The right-hand side of Equation (11) can be easily computed for uniform random variables using the following result.

**Result 1:** For a uniform random  $X$  defined on the interval  $[c, d]$

$$\begin{aligned} Pr[a < X < b] &= [(b - c)^+ - (a - c)^+ - (b - d)^+ \\ &\quad + (a - d)^+]/(d - c), \end{aligned} \quad (12)$$

where  $x^+ = \max(0, x)$ , that is, for all real  $x$ ,  $x^+$  is zero if  $x \leq 0$  and simply  $x$  if  $x > 0$ .

Result 1 can be shown to hold true by exhausting all the possible locations of  $a, b$  with respect to  $c, d$ .

Since  $R^2$  in general will not have a uniform distribution, we cannot apply Result 1 directly to Equations (11), but by transforming  $R^2$  to a uniform random variable using Result 2 (Hogg and Tannis 1983), we can apply Equation (12).

**Result 2:** Let  $X$  be a random variable such that  $c < X < d$  with continuous probability density function  $p(x)$  and with strictly increasing, cumulative distribution function  $F(x) = \int_c^x p(r)dr$ . Then the random variable, defined by  $Y = F(X)$ , has a uniform distribution on  $[0, 1]$ .

Result 2 is useful because it says, for any random variable  $X$ , in order to compute  $Pr[c \leq X \leq x]$ , transform the inequality as follows,  $Pr[c \leq X \leq x] = Pr[F(c) \leq F(X) \leq F(x)]$ , and then apply Result 1.

$R$  is a random variable with cumulative distribution function, see Equation (3),

$$\begin{aligned} G_{\text{plug}}(x) &= \int_{r_a}^x p_{\text{gen}}(r)dr \\ &= \frac{2\pi}{Q_a} U_0(x^2/2 - r_a^2/2), \\ &\quad r_a \leq x \leq r_2. \end{aligned} \quad (13)$$

Thus by Result 2,  $G(R) = \frac{2\pi}{Q_a} U_0(R^2/2 - r_a^2/2)$  is uniform on  $[0, 1]$ . Thus, the transfer function for plug flow can be computed by transforming the inequality on the right-hand side of Equation (11) by adding  $-r_a^2$ , dividing by 2, multiplying by  $2\pi U_0/Q_a$ , on both sides of the inequalities, and then applying Result 1 as done below:

$$\begin{aligned} \Omega(Z_p \Delta\Phi_0) &= Pr\left[\frac{2\pi}{Q_a}[U_0(r_1^2/2 - r_a^2/2) - Z_p \Delta\Phi_0] \right. \\ &\quad \left. < G(R) < \frac{2\pi}{Q_a}[U_0(r_b^2/2 - r_a^2/2) - Z_p \Delta\Phi_0]\right] \\ &= \frac{2\pi}{Q_a} [((Q_c + Q_a)/2\pi + Z_p \Delta\Phi_0)^+ \\ &\quad - (Q_m/2\pi + Z_p \Delta\Phi_0)^+ \\ &\quad - (Q_c/2\pi + Z_p \Delta\Phi_0)^+ \\ &\quad + ((Q_m - Q_a)/2\pi + Z_p \Delta\Phi_0)^+]. \end{aligned} \quad (14)$$

In the last equality,  $U_0(r_1^2/2 - r_a^2/2) = -Q_c/2\pi$  and  $U_0(r_b^2/2 - r_a^2/2) = -(Q_m - Q_a)/2\pi$ , where  $Q_c, Q_m$  are the sheath air flow rate and the excess flow rate, respectively.

This expression for the transfer function is equivalent to the expression of Knutson and Whitby, but is written more succinctly and is easier to apply. Stolzenburg (1988) also simplifies Knutson's and Whitby's expression for the transfer function using the relation  $|a + b| + |a - b| = 2 \max(|a|, |b|)$  and derives the above expression for  $\Omega(Z_p \Delta\Phi_0)$ .

The same steps done for plug flow can be applied to all laminar, axisymmetric, and incompressible flows. Indeed, since  $E_z = 0$  and

$E_r = -V_0/r \ln(k)$ , Equations (1 and 2) can be written as follows:

$$\frac{dr}{dt} = u_r(r, z) - \frac{Z_p V_0 / \ln(k)}{r}, \quad (15)$$

$$\frac{dz}{dt} = u_z(r, z) \quad (16)$$

$$(r(0), z(0)) = (R, 0).$$

In order to use Results 1 and 2, transform the trajectory  $(r(t), z(t))$  as follows,

$$y(t) = G(r(t), z(t)), \quad (17)$$

for some twice differentiable (both variables) function;  $G(r, z)$  to be specified later. The transformed trajectory,  $y(t)$ , satisfies the following differential equation,

$$\frac{dy}{dt} = \frac{\partial G}{\partial r} \frac{dr}{dt} + \frac{\partial G}{\partial z} \frac{dz}{dt}, \quad y(0) = G(R, 0),$$

or equivalently the integral equation

$$y(t) = G(R, 0) + \int_0^t \frac{\partial G}{\partial r}(r(s), z(s)) u_r(r(s), z(s)) ds$$

$$- \frac{Z_p V_0}{\ln(k)} \int_0^t \frac{\partial G}{\partial r}(r(s), z(s)) \frac{1}{r(s)} ds$$

$$+ \int_0^t \frac{\partial G}{\partial z}(r(s), z(s)) u_z(r(s), z(s)) ds.$$

Now, freely choose  $G(r, z)$  such that

$$\frac{1}{r} \frac{\partial G}{\partial r}(r, z) = u_z(r, z) \frac{2\pi}{Q_a}, \quad (18)$$

then the second integral becomes  $-\frac{Z_p V_0}{\ln(k)} z(t) \frac{2\pi}{Q_a}$ , the first integral becomes

$$\frac{2\pi}{Q_a} \int_0^t r(s) u_z(r(s), z(s)) u_r(r(s), z(s)) ds,$$

and the third integral stays the same. If  $\frac{\partial G}{\partial z}(r, z)$ , is chosen such that

$$\frac{\partial G}{\partial z}(r, z) = -r u_r(r, z) \frac{2\pi}{Q_a},$$

then the first and third terms cancel one another and one gets the equation

$$G(r(t), z(t)) = G(R, 0) - \frac{Z_p V_0}{\ln(k)} z(t) \frac{2\pi}{Q_a}.$$

That there is such a well-defined function  $G(r, z)$  satisfying the above conditions follows from the incompressible condition of the air flow, that is,  $\frac{\partial G}{\partial z} r u_z(r, z) = -\frac{\partial G}{\partial r} r u_r(r, z)$ . The following equation is satisfied:

$$G(r(\tau), L) = G(R, 0) - \frac{Z_p V_0}{\ln(k)} L \frac{2\pi}{Q_a}.$$

Using Equation (18), take  $G(r, z) = \frac{2\pi}{Q_a} \int_{r_a}^r x u_z(x, z) dx$ . Note that for  $r_a < r < r_b$

$$\frac{\partial G}{\partial r}(r, 0) = (r u_z(r, 0)) \frac{2\pi}{Q_a} = p_{\text{gen}}(r);$$

see Equation (3). Thus integrating

$$G(r, 0) = \int_{r_a}^r p_{\text{gen}}(x) dx$$

and by Result 2,  $G(R, 0)$  is a uniform (0,1) random variable.

Since  $G(r, L)$  is a nondecreasing function of  $r$ , the following calculations hold:

$$\Omega(Z_p \Delta \Phi_0)$$

$$= Pr[r_1 < r(\tau) < r_b]$$

$$= Pr[G(r_1, L) < G(r(\tau), L) < G(r_b, L)]$$

$$= Pr \left[ G(r_1, L) + \frac{Z_p V_0}{\ln(k)} L \frac{2\pi}{Q_a} \right.$$

$$\left. < G(R, 0) < G(r_b, L) \right.$$

$$\left. + \frac{Z_p V_0}{\ln(k)} L \frac{2\pi}{Q_a} \right]$$

$$= Pr \left[ -\frac{2\pi}{Q_a} \frac{Q_c}{2\pi} - Z_p \Delta \Phi_0 \frac{2\pi}{Q_a} < G(R, 0) \right.$$

$$\left. < -\frac{2\pi}{Q_a} \frac{Q_m - Q_a}{2\pi} - Z_p \Delta \Phi_0 \frac{2\pi}{Q_a} \right].$$

As in the calculations for plug flow, see Equation (14); by applying Result 2, this equation reduces to the Knutson-Whitby transfer function.

### EFFECTS OF BROWNIAN MOTION

As a result of random collisions between the aerosol particles and the air molecules, aerosol particles undergo diffusion. Diffusion is reflected in the aerosol particle's trajectory as a random perturbation. These perturbations are described by Brownian motion. The probability  $p(x, t)$  that at time  $t$  the perturbation is of length  $x$  is given by  $p_D(x, t) = \frac{1}{\sqrt{2\pi Dt}} \exp\{-x^2/4Dt\}$ , where  $D$  denotes the diffusion coefficient. For spherical particles  $D = k_b T C(d_p) / 3\pi \mu d_p$ , where  $k_b$  is Boltzmann's constant,  $T$  is temperature,  $C(d_p)$  is the Cunningham slip correction, and  $\mu$  denotes viscosity.

Introduce the variable  $x(t) = \sqrt{2D}B(t)$ , where  $B(t)$  is standard Brownian motion, and the increment  $B(t + \Delta) - B(t)$  is a mean zero Gaussian random variable with variance equal to  $\Delta$ . Then, the variance of the random displacement due to Brownian motion satisfies

$$\text{Var}[x(t + \Delta) - x(t)] = 2D\Delta$$

and has density  $p_{D\Delta}(x, t)$ . Let  $(B_x(t), B_y(t), B_z(t))$  denote 3-D standard Brownian motion, independent of  $R$ ; then the equations of motion in rectangle coordinates,  $(x(t), y(t), z(t))$ , of the aerosol particles are given by

$$\begin{aligned} dx &= [u_x(x, y, z) + Z_p E_x(x, y, z)]dt \\ &\quad + \sqrt{2D} dB_x(t), \\ dy &= [u_y(x, y, z) + Z_p E_y(x, y, z)]dt \\ &\quad + \sqrt{2D} dB_y(t), \\ dz &= [u_z(x, y, z) + Z_p E_z(x, y, z)]dt \\ &\quad + \sqrt{2D} dB_z(t). \end{aligned} \quad (19)$$

It is convenient to orient an  $xyz$  coordinate system so that the  $yz$  plane contains the particle trajectory; that is,  $z$  is at the center of the collection

rod,  $y$  is equivalent to the radial position of the particle, and  $x$  is nominally zero except for the contribution from Brownian motion. Provided the minimum value of  $y$  is large compared to a diffusion length scale, the 3-D trajectory reduces to a two-dimensional (2-D)  $yz$  trajectory defined by the last two of the three expressions given in Equation (19). In the Appendix it is shown for plug flow that the 3-D trajectory in cylindrical coordinates can be accurately represented by a 2-D trajectory, provided the minimum value of  $y$ ,  $y_{\min}$ , satisfies the following equation:

$$y_{\min} \gg \sqrt{(DL/2U_0)}. \quad (20)$$

For the DMA configured as described above,  $y_{\min}$  is approximately 1 cm and the quantity on the right-hand side (RHS) of the equation corresponding to the diffusion coefficient of a 1 nm sphere is about 0.25 cm. So even in this extreme case of a 1 nm sphere, the condition in Equation (20) is satisfied. A condition for parabolic flow is also given in the Appendix. For notational convenience we use  $r$  rather than  $y$ , noting that in two dimensions,  $y$  and the radial variable are identical. The basic reasons for the simplification from 3-D to 2-D are that the motion is independent of the azimuthal angle (see Appendix) and that the diffusional motion is small compared to electric field induced motion. The resulting equations are given by

$$\begin{aligned} dr &= [u_r(r, z) + Z_p E_r(r, z)]dt \\ &\quad + \sqrt{2D} dB_r(t), \\ dz &= [u_z(r, z) + Z_p E_z(r, z)]dt \\ &\quad + \sqrt{2D} dB_z(t). \end{aligned}$$

We shall not treat the Brownian motion problem in its full generality, but shall assume that  $u_r(r, z) = 0$ ,  $u_z(r, z) = u_z(r)$ . This simplification includes many useful flows, e.g., plug flows, viscous flows through a cylinder, flows through an annular region, etc.

Under these modifications, the equations of  $r(t)$  and  $z(t)$  reduce to

$$dr = \frac{-Z_p V_0 / \ln(k)}{r} dt + \sqrt{2D} dB_r(t), \quad (21)$$

$$dz = u_z(r)dt + \sqrt{2D} dB_z(t). \quad (22)$$

Even for simple plug flow, solving the system of Stochastic Differential Equations (21) and (22) in closed form is not possible. The method we take is to solve the Stochastic Differential Equations (21) and (22) for the trajectories, directly, using a weighted Monte-Carlo method. Then the transfer function

$$\Omega(Z_p \Delta \Phi_0) = Pr[r_1 < r(\tau) < r_b]$$

is calculated as described below for both plug flow and parabolic flow. Other methods, notably Stolzenburg's, result in analytic approximations for the transfer function. The Monte-Carlo simulations are compared to Stolzenburg's results.

### STOLZENBURG'S RESULTS

Stolzenburg's (1988) analysis starts by writing the position vector in terms of the curvilinear coordinates:  $s$  the arc length along the streamline and  $x$  the perpendicular distance from the streamline due to diffusion. Then, the aerosol velocity vector is expanded into a first-order Taylor series expansion about  $x = 0$ . With additional simplifications, e.g., neglecting wall losses, the problem reduces to the diffusion of a one-dimensional (1-D) Brownian particle in an infinite medium. Stolzenburg's transfer function is a convolution of the nondiffusive transfer function with a Gaussian distribution and is given by

$$\begin{aligned} \Omega(\tilde{V}) = \frac{\sigma}{\sqrt{2}\beta} & \left[ \epsilon \left( \frac{\tilde{V} - (1 + \beta)}{\sqrt{2}\sigma} \right) \right. \\ & + \epsilon \left( \frac{\tilde{V} - (1 - \beta)}{\sqrt{2}\sigma} \right) \\ & \left. - 2\epsilon \left( \frac{\tilde{V} - 1}{\sqrt{2}\sigma} \right) \right], \quad (23) \end{aligned}$$

where

$$\epsilon(x) = x \operatorname{erf}(x) + \frac{1}{\sqrt{\pi}} \exp(-x^2),$$

$$\beta = Q_a / Q_c,$$

$$\tilde{V} = V_0 / V_0^*,$$

$$V_0^* = \frac{Q_c \ln(r_1 / r_2)}{2\pi LZ_p},$$

$$\sigma^2 = G\tilde{D},$$

$$\tilde{D} = \frac{2\pi LD}{Q_c},$$

$$G = \frac{4(1 + \beta)^2}{1 - \gamma} [I_\gamma(\gamma) + (2(1 + \beta)\kappa)^{-2}],$$

$$\gamma = (r_1 / r_2)^2,$$

$$\kappa = Lr_2 / (r_2^2 - r_1^2)$$

for plug flow

$$I_\gamma(\gamma) = \frac{1}{2}(1 + \gamma)$$

and for inviscid flow

$$\begin{aligned} I_\gamma(\gamma) = & \frac{\left[ \frac{1}{4}(1 - \gamma^2)(1 - \gamma)^2 + \frac{5}{18}(1 - \gamma^3)(1 - \gamma) \right. \\ & \left. \times \ln(\gamma) + \frac{1}{12}(1 - \gamma^4) \cdot \ln^2(\gamma) \right]}{\left[ (1 - \gamma) \left[ -\frac{1}{2}(1 + \gamma) \cdot \ln(\gamma) - (1 - \gamma)^2 \right] \right]^{-1}}. \end{aligned}$$

We have used the dimensionless voltage  $\tilde{V}$  as the independent variable, since in our simulation the particle mobility is fixed and the voltage is varied. This set of equations was used in computing the transfer function for comparison with the Monte-Carlo results. There are two limiting results that are useful for comparing the overall behavior of the transfer function. One is the peak value of the transfer function,  $\Omega(\tilde{V} = 1)$ , as a function of  $\beta$  and  $\sigma$  and the other is the standard deviation,  $S(\tilde{V})$ , of the reduced electrical mobility. Setting  $\tilde{V} = 1$  in Equation (23), one obtains

$$\begin{aligned} \Omega(\tilde{V} = 1) & = \frac{1}{w} (\epsilon(w) - \epsilon(0)) \\ & = \operatorname{erf}(w) - \frac{1}{w\sqrt{\pi}} (1 - \exp(-w^2)), \quad (24) \end{aligned}$$

where  $w = \frac{\beta}{\sqrt{2\sigma}}$ . Next we write the expression for the standard deviation given by Stolzenburg:

$$S(\tilde{V} = 1) = \left[ \frac{1}{6} \beta^2 + \sigma^2 (1 + 2\sigma^2) \right]^{1/2} \\ = S_{nd} \left[ 1 + \frac{3}{w^2} (1 + 2\sigma^2) \right], \quad (25)$$

where  $S_{nd}$  is the standard deviation in the absence of diffusion. For particle sizes larger than 3 nm, the  $\sigma$  term is small so that the standard deviation can be approximated by

$$S(\tilde{V} = 1) = S_{nd} \left[ 1 + \frac{3}{w^2} \right]^{1/2}.$$

We see that both the peak in the transfer function and the standard deviation of the reduced mobility are functions of  $w$ , which is proportional to  $\beta/\sigma$ . For sheath flow of 166.7 cm<sup>3</sup>/s and the DMA dimensions given above one obtains the following expression for  $w$ :

$$w = \frac{c\beta}{(1 + \beta)\sqrt{D}},$$

where  $c$  is a constant equal to 0.3055 with dimensions cm/ $\sqrt{s}$ ,  $D$  is the diffusion coefficient, and cm and s refer to the units of centimeters and seconds. So this analysis will fully define the unit performance for a fixed sheath flow. For other sheath flows the explicit expression would change, since as indicated in the equation,  $\tilde{D}$  is inversely proportional to the sheath flow rate. Of course, if the geometry changes, this would change both the flow function  $G$  and  $\tilde{D}$ . To minimize the effects of diffusion, one wants to reduce the residence time in the DMA by increasing the flow rate and/or decreasing the length of the classifier.

**Monte-Carlo:** The Stochastic Differential Equations (21) and (22) were solved using an Euler solver in conjunction with a Monte-Carlo simulation, i.e., let

$$r(t + \Delta t) = r(t) - \frac{Z_p V_0 / \ln(k)}{r(t)} \Delta t + a(t), \quad (26)$$

$$z(t + \Delta t) = z(t) + u_z(r(t)) \Delta t + b(t), \quad (27)$$

where  $a(t)$  and  $b(t)$  denote independent increments of Brownian motions, i.e., Gaussian random variables with means zero and root mean square (RMS) given by

$$\sqrt{E[a^2(t)]} = \sqrt{2D\Delta t},$$

$$\sqrt{E[b^2(t)]} = \sqrt{2D\Delta t},$$

where  $\Delta t$  is the time step of the simulation (Kloeden and Platen 1992).  $\Delta t$  was set at 0.002 s for the simulations.  $u_z$  is the axial velocity which is obtained either as a constant for the inviscid flow or as a parabolic function of radial location for the viscous flow. The inlet region of the aerosol is a concentric cylinder with inner radius  $r_a$  and outer radius  $r_2$ . The area,  $\pi(r_2^2 - r_a^2)$ , corresponds to the area required for the aerosol flow with the given velocity profile. This area is divided into 100 concentric rings, and the volume flow of the aerosol through each ring is calculated. For any voltage  $V_0$ , the particle trajectories are started from the center of each ring with a weight equal to the fraction of aerosol flow through that ring. 200 particles are started from each ring, and the particle trajectory is terminated if the particle touches either the inner ( $r_1$ ) or outer ( $r_2$ ) wall. If the particle does not touch either wall, its radial location at the outlet boundary  $z = L$  is obtained. If this radial location is smaller than the outlet port ( $r_b$ ), then the particle passes through the counter and its weight is added to a running total.  $r_b$  is obtained by finding out the area required for the entire aerosol flow to pass between the inner rod  $r_1$  and  $r_b$ . This total is divided by 200 at the end of the simulation to yield the transfer function for the particular voltage.

For the viscous flow, the mass flux through a ring was obtained by multiplying the cross-sectional area of the ring by the local velocity profile,  $u_z(r)$ , given in Equation (7). Then the probability of any particle starting at a specific radial ring is obtained by dividing the local mass flux by the total mass flux of particles. This is

the weight given to each trajectory used in a weighted Monte-Carlo simulation.

We now analyze the Monte-Carlo results. The effect of diffusion on the transfer function for two flow settings of the classifier is considered: a commonly used 10:1 flow ratio and a high resolution 40:1 flow ratio. The high resolution flow ratio is used for measuring the widths of the size distribution of monodisperse polystyrene spheres (Mulholland et al. 1996, Kinney et al. 1991). The transfer functions of two flow profiles (a plug flow and a viscous flow) are considered.

Also, it is possible to solve for the transfer function by setting up a boundary value problem using Dynkin's equation, which leads to a partial differential equation representation of the transfer function (Schuss 1980). This approach was taken by Hagwood et al. (1995).

## RESULTS

Sample trajectories obtained with and without taking into account the random component are shown in Figure 5 for a 100 nm diameter particle for plug flow. The two sample trajectories influenced by diffusion terminate near the edge of the outlet slit, while the trajectory without diffusion terminates at the center of the outlet slit. Thus it is not surprising that the peak value of transfer function will be reduced as a result of this diffusion process.

The transfer function for the 100 nm particles is plotted in Figure 6 for the 10:1 flow ratio. It is seen that in this case diffusion has very little effect on the transfer function. However, for the 30 nm particles the peak value of the transfer function decreases from about 1 to about 0.88 as a result of the particle diffusion, as shown in Figure 7. It is also seen that the trans-

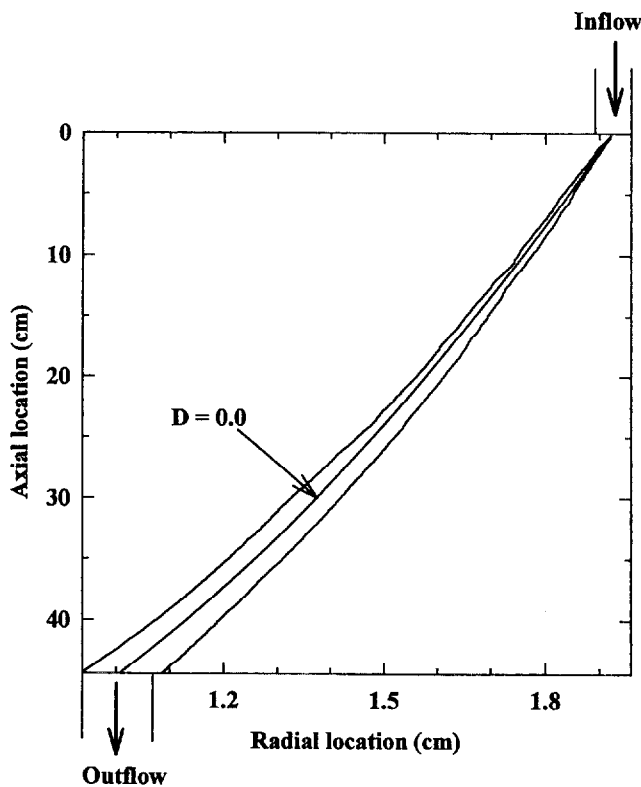


FIGURE 5. The effect of diffusion on the central trajectory in a DMA classifier with plug flow and at a 10:1 flow ratio for the 100 nm particles.

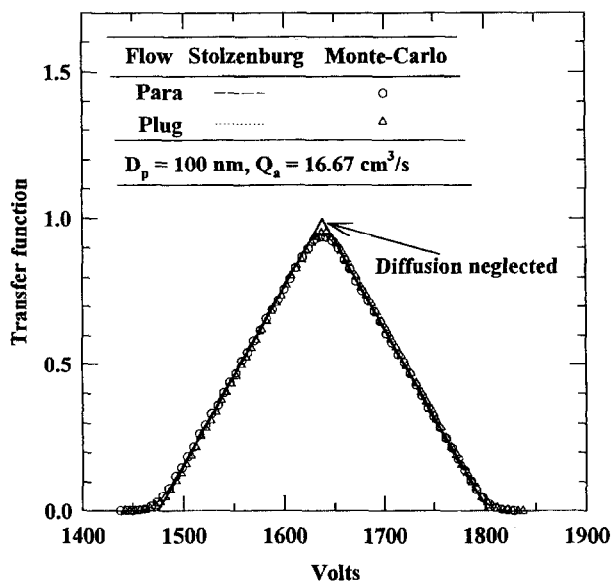


FIGURE 6. The transfer function for a DMA classifier with 100 nm particles, 166.7 cm<sup>3</sup>/s of sheath air, and 16.67 cm<sup>3</sup>/s of aerosol flow.

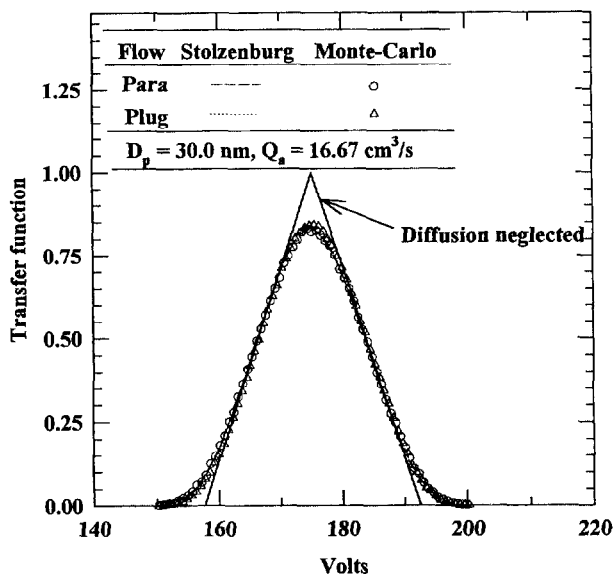


FIGURE 7. The transfer function for a DMA classifier with 30 nm particles, 166.7 cm<sup>3</sup>/s of sheath air, and 16.67 cm<sup>3</sup>/s of aerosol flow.

fer function for both the plug and the viscous flows are almost identical. Also, the Monte-Carlo calculation and Stolzenburg's result (Equation (23)), were almost identical.

To obtain accurate size distributions it is important to operate the classifier at a high ratio of sheath to aerosol flow rate. Sample trajectories

for the 30 nm particle and for a 40:1 flow ratio are plotted in Figure 8. In this case it can be seen that the sample trajectories miss the outlet slit by a wide margin, indicating a greater diffusional effect on the transfer function. Figures 9 and 10 give the transfer functions for the 100 nm and 30 nm particles at this high flow ratio. It is seen

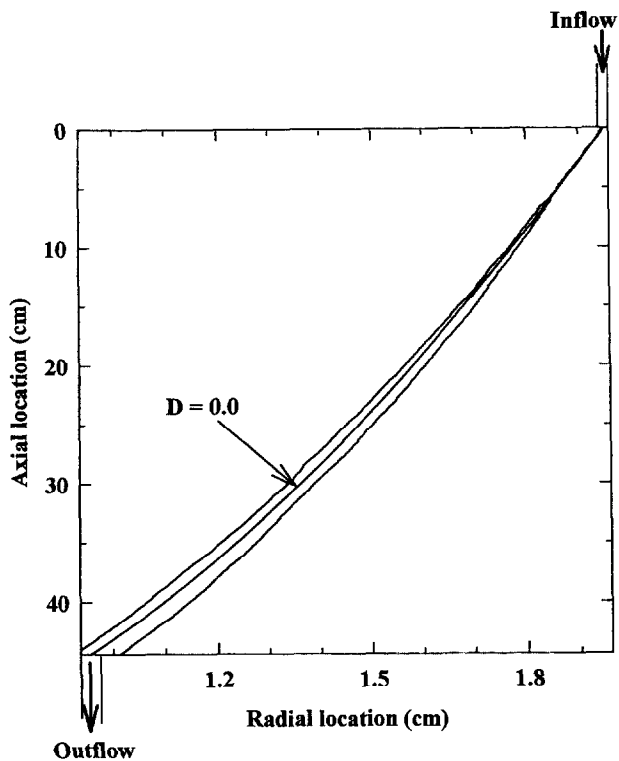


FIGURE 8. The effect of diffusion on the central trajectory in a DMA classifier with plug flow and at a 40:1 flow ratio.

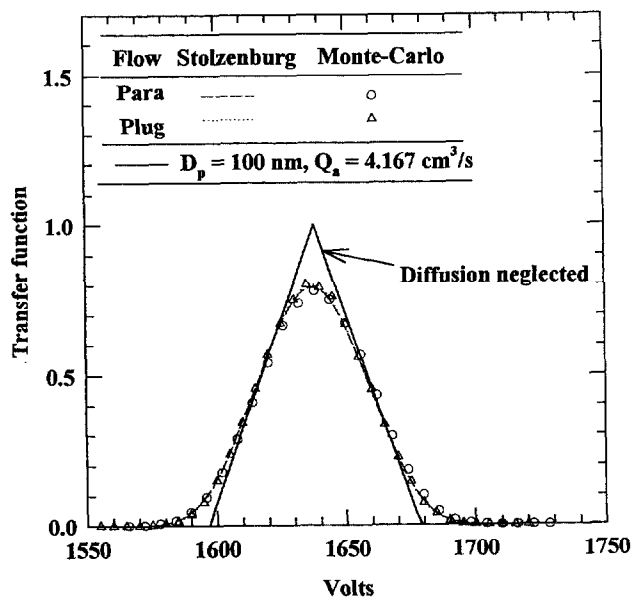


FIGURE 9. The transfer function for a DMA classifier with 100 nm particles, 166.7 cm<sup>3</sup>/s of sheath air, and 4.167 cm<sup>3</sup>/s of aerosol flow.

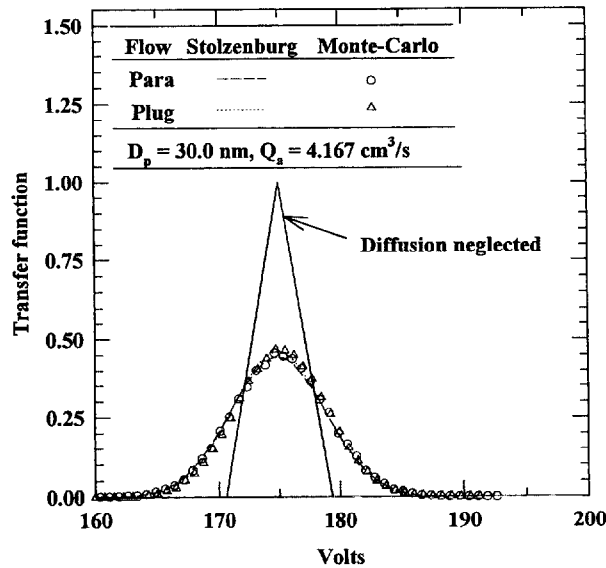


FIGURE 10. The transfer function for a DMA classifier with 30 nm particles, 166.7 cm<sup>3</sup>/s of sheath air, and 4.167 cm<sup>3</sup>/s of aerosol flow.

that the peak values of the transfer function are significantly reduced in both cases. Comparing Figures 7 and 10, we can see that for the same particle size, diffusion has a greater impact on the higher flow ratio case. Quantitatively, the reason is that the outlet target area for the particles is smaller for the higher flow ratios. Using a triangular transfer function would result in a significant error for particles of 100 nm or less for these high flow ratios. The fact that both the viscous and plug flow cases show similar results indicates that the present conclusions are not dependent on the particular flow profile. Again it is seen that the Monte-Carlo calculations are essentially identical to the results from Stolzenburg's analysis.

Monte-Carlo calculations were carried out for particle sizes 10 nm, 3 nm, and 1 nm to determine at what size the assumptions of no wall loss affects Stolzenburg's results. The results for the 10 nm particles are given in Figures 11 and 12. The first discrepancy between the theory and the Monte-Carlo simulations is evident for the 4.167 cm<sup>3</sup>/s flow rate. It can be seen that for this particular flow rate, the Monte-Carlo simulations show a greater diffusion effect for

the plug flow case as compared to the parabolic case. In addition, there is a skewness of the profile. For the plug flow, the flux of particles that pass very close to the wall is higher than for the parabolic flow. Therefore, for small particle sizes and small exit orifices, the number of particles that impinge on the wall is higher for the plug flow, reducing the transfer function. It is noted that such affects were not present for the larger particles, since the wall losses are almost negligible.

The skewness for the low voltages could be due to the effect of lower radial velocities at low voltages. The diffusion "velocities" relative to the radial velocity leads to increased wall loss. This produces a significant skewness to the transfer function.

For the 3 nm particle size, the reduction in the transfer function for the plug flow relative to the parabolic flow becomes more apparent as indicated in Figures 13 and 14. For the case of the aerosol flow of 4.167 cm<sup>3</sup>/s, the Stolzenburg results overestimate the peak in the transfer function by a factor of about 2. Because of the large diffusion coefficient, the width of the transfer function at this flow rate is only slightly

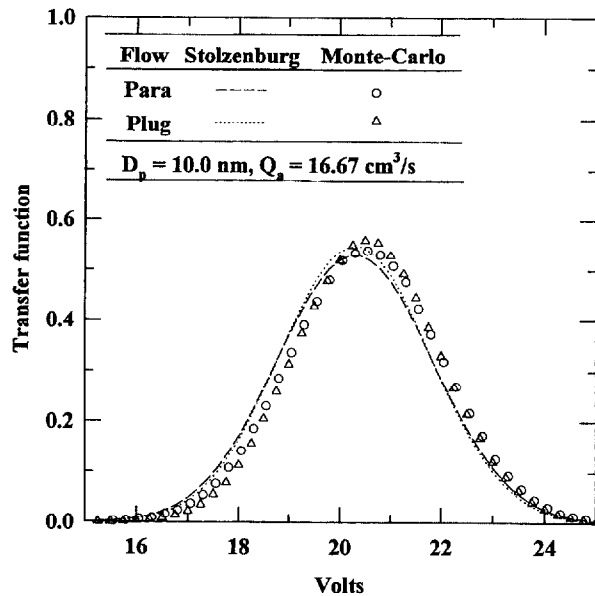


FIGURE 11. The transfer function for a DMA classifier with 10 nm particles, 166.7 cm<sup>3</sup>/s of sheath air, and 16.67 cm<sup>3</sup>/s of aerosol flow.

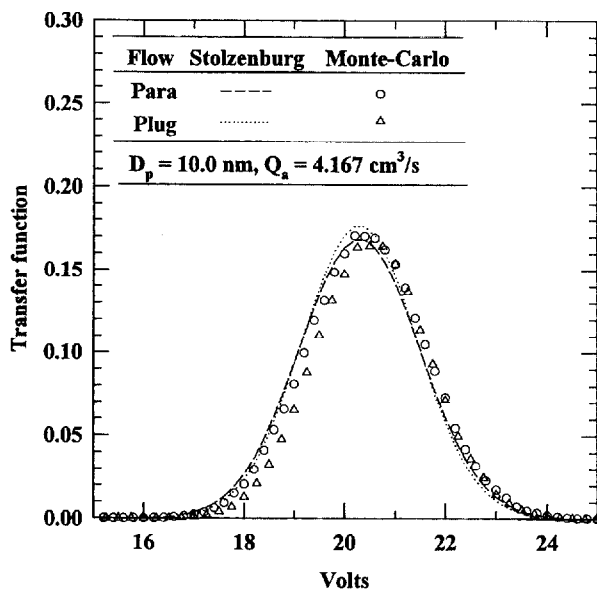


FIGURE 12. The transfer function for a DMA classifier with 10 nm particles, 166.7 cm<sup>3</sup>/s of sheath air, and 4.167 cm<sup>3</sup>/s of aerosol flow.

smaller than the case for an aerosol flow rate that is four times larger. For the 100 nm particle size the width of the transfer function for the smaller flow was narrower than the larger flow by a factor of 4.

The Monte-Carlo results for the 1 nm particles shown in Figures 15 and 16 are a factor of 3 to 30 lower than the Stolzenburg results. The wall loss becomes a dominant effect for this particle size and DMA configuration. Monte-Carlo

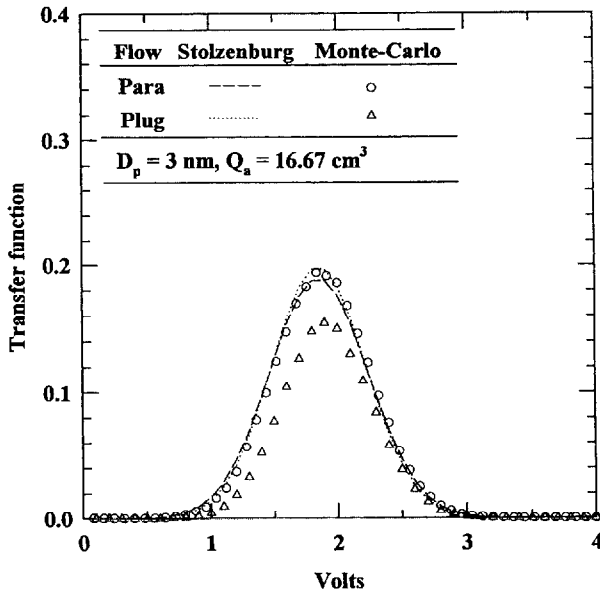


FIGURE 13. The transfer function for a DMA classifier with 3 nm particles, 166.7 cm<sup>3</sup>/s of sheath air, and 16.67 cm<sup>3</sup>/s of aerosol flow.

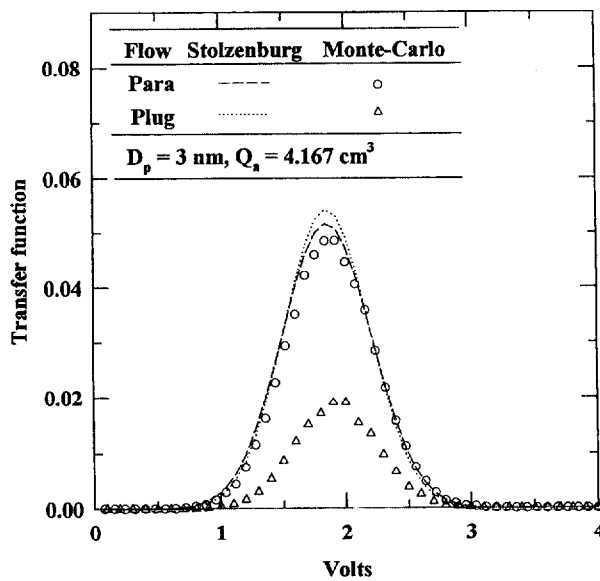


FIGURE 14. The transfer function for a DMA classifier with 3 nm particles, 166.7 cm<sup>3</sup>/s of sheath air, and 4.167 cm<sup>3</sup>/s of aerosol flow.

simulations including axial diffusion were also carried out, and the results were essentially the same as those without axial diffusion.

Two graphical summaries of the calculations are contained in Figures 17 and 18. From the

plot of the peak in the transfer function versus diameter, it is seen that there is good agreement between the Monte-Carlo results and Stolzenburg's analysis for particle diameters of 10 nm and larger. It is apparent that the agreement is

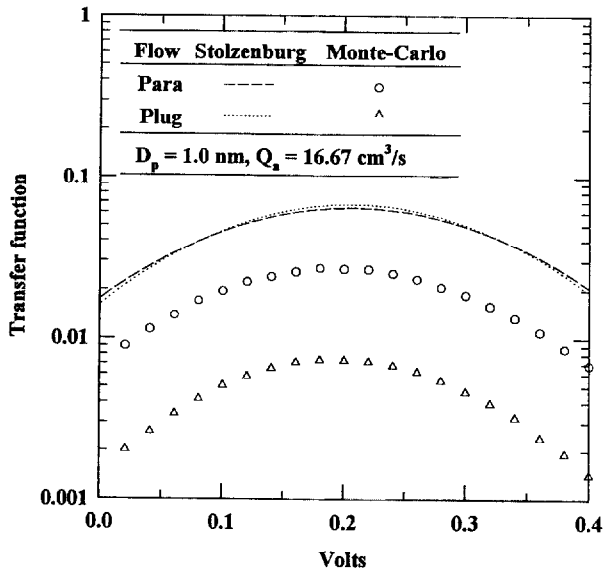


FIGURE 15. The transfer function for a DMA classifier with 1 nm particles, 166.7 cm<sup>3</sup>/s of sheath air, and 16.67 cm<sup>3</sup>/s of aerosol flow.

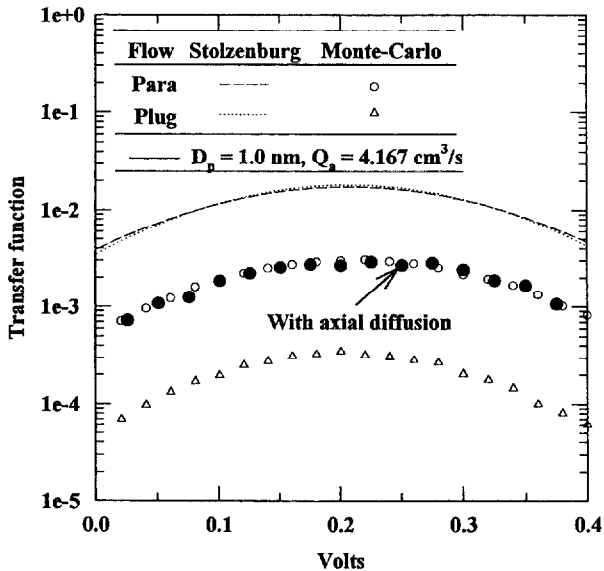


FIGURE 16. The transfer function for a DMA classifier with 1 nm particles, 166.7 cm<sup>3</sup>/s of sheath air, and 4.167 cm<sup>3</sup>/s of aerosol flow. The solid circles refer to the Monte-Carlo simulation with axial diffusion included.

much better for the parabolic flow than for the plug flow.

Figure 18 provides a comparison of the reduced width of the transfer function with particle diameter. The results include the Monte-Carlo simulations, the moment analysis of Equation (23), and the simplified expression obtained

by Stolzenburg, Equation (25). It is seen that the standard deviation is more sensitive to wall loss than the peak with a small difference observed between the Monte-Carlo simulation and Stolzenburg's results for the 30 nm particles with the low flow ratio. The difference increases with decreasing size. Surprisingly, the approxi-

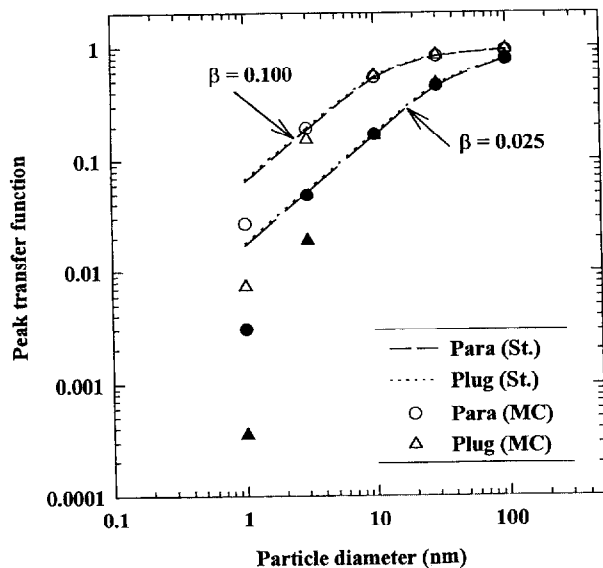


FIGURE 17. Comparison of the peaks in the transfer functions with particle diameters for the Monte-Carlo results (MC) and Equation (24) from Stolzenburg's results (St.) for flow ratios of 0:1 and 0:025.

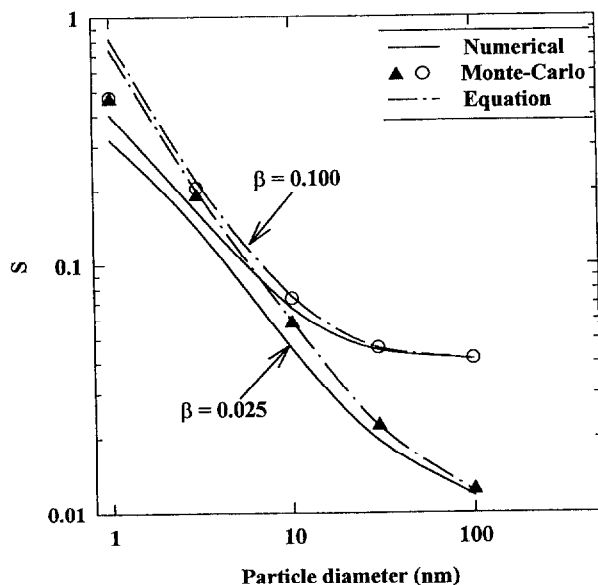


FIGURE 18. Comparison of reduced standard deviations from the Monte-Carlo results, numerical determination of moments using Equation (23), and Equation (25) for the case of parabolic flow.

mate formula derived by Stolzenburg agrees better with the Monte-Carlo simulation with significant difference only apparent for the 1 nm particle size. It is important to comment that our analysis is based on a monodisperse particle size. Stolzenburg obtains a somewhat different result based on analyzing Equation (23) for

a fixed voltage but a range of particle diameters/mobilities.

The preceding results are based on a classifier of length 44 cm. Recently, classifiers have been fabricated with lengths reduced by a factor of 4 and by a factor of 16. In these cases the diffusion broadening will have less impact. The

broadening for a 10 nm diameter particle for a full length classifier equals the broadening for a 5 nm diameter particle for a 1/4 length classifier and equals the broadening for about a 2.5 nm diameter particle for a 1/16 length classifier.

## CONCLUSION

1. The effect of particle diffusion on the DMA transfer function can be conveniently assessed by using Monte-Carlo simulations without having to neglect axial diffusion or wall losses.
2. The Stolzenburg analysis, which neglects wall losses, agrees with the Monte-Carlo results for particle diameters larger than 10 nm for an aerosol to sheath flow ratio ( $\beta$ ) of 0:1.
3. For particle sizes smaller than 10 nm and  $\beta = 0.1$ , the Monte-Carlo method indicates large wall losses resulting in reduction in the transfer function by as much as a factor of 10 to 30, sensitivity to the flow field, and skewness of the transfer function. For the case where  $\beta = 0.025$ , a small effect on the width of the transfer function is already apparent for a particle diameter of 30 nm.

## APPENDIX

If the motion is written in rectangular coordinates as in Equation (19), then the radial location  $r(t)$  satisfies  $r(t) = \sqrt{x^2(t) + y^2(t)}$ , so by a change of variables using Ito's formula, see below:

$$\begin{aligned} dr &= \left[ u_r(r, z) + Z_p E_r(r, z) + \frac{D}{r} \right] dt \\ &\quad + \sqrt{2D} [\cos(\theta) dB_x(t) + \sin(\theta) dB_y(t)] \\ &= \left[ u_r(r, z) + Z_p E_r(r, z) + \frac{D}{r} \right] dt \\ &\quad + \sqrt{2D} dB_r(t), \end{aligned} \quad (28)$$

where  $B_r(t)$  denotes 1-D Brownian motion and  $\theta$  is the azimuthal angle. That  $\cos(\theta) dB_x(t) +$

$\sin(\theta) dB_y(t)$  is Brownian motion is also shown. Since  $u_r$  and  $E_r$  are independent of  $\theta$  and because of the geometry of the DMA, in cylindrical coordinates the motion is independent of the azimuthal angle. So, if the term  $(D/r)dt$  is negligible, the motion can be described by the Brownian perturbation model

$$\begin{aligned} dr &= [u_r(r, z) + Z_p E_r(r, z)] dt \\ &\quad + \sqrt{2D} dB_r(t), \end{aligned} \quad (29)$$

$$\begin{aligned} dz &= [u_z(r, z) + Z_p E_z(r, z)] dt \\ &\quad + \sqrt{2D} dB_z(t). \end{aligned} \quad (30)$$

To measure the importance of the term  $(D/r)dt$ , consider a particle that travels at an average axial velocity  $\bar{v}$ . At this velocity, it takes time  $L/\bar{v}$  to traverse distance  $L$  in the  $z$  direction. During this time,  $B_r(t)$  will perturb the distance traveled by an amount of  $\sqrt{2DL/\bar{v}}$  and the displacement associated with the term  $(D/r)dt$  will always be less than  $DL/r_1\bar{v}$ , thus the displacement due to  $(D/r)dt$  will be small compared to Brownian motion if

$$DL/r_1\bar{v} \ll \sqrt{2DL/\bar{v}}.$$

For plug flow  $\bar{v} = U_0$  and the term  $(D/r)dt$  is negligible provided  $r_1 \gg \sqrt{DL/2U_0}$ . For parabolic flow  $\bar{v} = Q_c/(\pi(r_2^2 - r_1^2))$  and the term  $D/r$  is negligible if  $r_1^2/(r_2^2 - r_1^2) \gg DL\pi Q_c$ ; the RHS is a measure of the fraction of  $r_1$  contained in the separation between the cylinders  $r_2 - r_1$ .

**Ito's formula:** For the change of variable rule for stochastic differential equations, Gard (1988) states that if  $y(t) = F(x_1(t), x_2(t), \dots, x_n(t))$ , where

$$\begin{aligned} dx_i(t) &= f_i(x_1(t), \dots, x_n(t))dt + \sigma_i dB_i(t), \\ i &= 1, \dots, n, \end{aligned}$$

then for every function  $F$  having continuous partial derivatives up to order two,

$$dy(t) = \left[ \sum_{i=1}^n f_i \frac{\partial F}{\partial x_i} + \sum_{i=1}^n \frac{1}{2} \sigma_i^2 \frac{\partial^2 F}{\partial x_i^2} \right] dt + \sum_{i=1}^n \sigma_i \frac{\partial F}{\partial x_i} dB_i(t).$$

For the example in section 4,  $F(x_1, x_2) = \sqrt{x_1^2 + x_2^2}$  and

$$\frac{\partial F}{\partial x_i} = \frac{x_i}{r},$$

$$\frac{\partial^2 F}{\partial x_i \partial x_j} = \frac{\delta_{ij}}{r} - \frac{x_i x_j}{r^3}.$$

**Brownian motion:** The reason  $\cos(\theta)dB_x(t) + \sin(\theta)dB_y(t) = dB_r(t)$  follows from the fact that  $dB_x(t) \approx B_x(t + \Delta t) - B_x(t)$ , thus it is independent of  $B_x(t)$  and thus of  $\theta = \theta(B_x(t), B_y(t))$ . A similar statement can be made for  $dB_y(t)$ . By conditioning on  $(B_x, B_y)$  and using the Markov property of Brownian motion, one can see that  $\cos(\theta)dB_x(t) + \sin(\theta)dB_y(t)$  is just Brownian motion.

---

*We would like to express our sincere gratitude for one of the referees, whose rigorous review made this a better paper.*

---

## References

- Chen, D. R., and Pui, D. Y. H. (1997). Numerical Modeling of the Performance of Differential Mobility Analyzers for Nanometer Aerosol Measurements, *accepted for publication in J. Aerosol Science*.
- Endo, Y., Fukushima, N., Tashiro, S., and Kousaka, Y. (1997). Performance of a Scanning Differential Mobility Analyzer, *Aerosol Sci. Technol.* 26: 43–50.
- Gard, T. C. (1988). *Introduction to Stochastic Differential Equations*. Marcel Dekker, Inc., New York, pp. 81–82.
- Hagwood, C., Coakley, K., Negiz, A., and Ehara, K. (1995). Stochastic Modeling of a New Spectrometer, *Aerosol Sci. Technol.* 23:611–627.
- Hogg, R. V. and Tanis, E. A. (1983). *Probability and Statistical Inference*. Macmillan, New York, p. 159.
- Kinney, P. O., Pui, D., Mulholland, G. and Bryner, N. (1991). Use of the Electrostatic Classification Method to Size 0.1  $\mu\text{m}$  SRM Particles-A Feasibility Study, *J. Res. Natl. Inst. Stand. Technol.* 96:147–176.
- Kloeden, P. E., and Platen E., (1992). *Numerical Solution of Stochastic Differential Equations*. Springer, Berlin, pp. 305–306.
- Knutson, E. O. and Whitby, K. T. (1975). Aerosol classification by Electric Mobility: Apparatus, theory and applications, *J. Aerosol Sci.* 6:443–451.
- Liu, B. Y. H., and Pui, D. Y. H. (1974). A Submicron Aerosol Standard and the Primary, Absolute Calibration of the Condensation Nuclei Counter, *J. Colloid and Interface Sci.* 47:155–171.
- Mulholland, G. W., Byrmer, N., Liggett, W., Scheer, B. W., and Goodall, R. K. (1996). *Proc. SPIE* 2862:104–118.
- National Institute of Standards and Technology (NIST). *Standard Reference Material 1963*, Standard Reference Material Program, NIST, Gaithersburg, MD.
- Ooghe, M., Mesbah, B., and Boulaud, D. (1994). Radial Flow Differential Mobility Analyzer, in *Abstracts from the Proc. 4th Int. Aerosol Conf.*, (Flagan, R.C., ed.), Los Angeles, California, August 29–September 2, pp. 463–464.
- Rosell-Llompарт, J., Loscertales, I. G., Bingham, D., and Fernández de la Mora, J. (1996). Sizing Nanoparticles and Ions with a Short Differential Mobility Analyzer, *J. Aerosol Sci.* 27:695–719.
- Schuss, A. (1980). *Theory and Applications of Stochastic Differential Equations*, John Wiley and Sons, New York.
- Stolzenburg, M. R. (1988). An Ultrafine Aerosol Size Distribution Measuring System, Ph.D. Thesis, University of Minnesota, Minneapolis.
- Tammiet, H. F. (1970). The Aspiration Method for the Determination of Atmospheric-Ion Spectra, *Israel Program for Scientific Translations, Jerusalem*. (Original work in Russian published in 1967.)
- Wang, S. C., and Flagan, R. C. (1990). Scanning Electrical Mobility Spectrometer, *Aerosol Sci. Technol.* 13: 230–240.
- Zhang, S. H., Akutsu, Y., Russell, L. M., Flagan, R. C., and Seinfeld, J. H. (1995). Radial Differential Mobility Analyzer, *Aerosol Sci. Technol.* 23: 357–372.

Received 1 May 1997; accepted 19 August 1998